HICUM/L2 version 2.23: Release Notes

M. Schroter, A. Mukherjee, A. Chakravorty

Chair for Electron Devices & Integrated Circuits (CEDIC)
University of Technology Dresden, Germany

Dept. of Electrical and Computer Engineering
University of California at San Diego, USA

Dept. of Electrical Engineering
Indian Institute of Technology, Madras, India

mschroter@ieee.org

http://www.iee.et.tu-dresden.de/iee/eb/comp_mod.html

September, 2008

Table of contents

1 Overview

This document contains for HICUM/L2 v2.23 the release notes in terms of important changes w.r.t. the former version 2.22 which was released in August 2006. In short, these changes comprise

- the implementation of vertical non-quasi-static (NQS) effects entirely in Verilog-A;
- the implementation of noise correlation between base and collector current in Verilog-A;
- few code related additions, bug fixes and optimizations.

These changes are indicated also in the Verilog-A code itself. The new version yields the same results as the previous version 2.22 except for the newly implemented NQS and noise correlation effects. In addition to this code release, an updated documentation will be released that incorporates all existing release notes and user feedback.

Reference code of HICUM/L2 v2.23 is available in Verilog-A and accessible at the web site given on the title page.

Important note:

The model is defined by the *code implementation* rather than by the documentation, which can not be *tested* for correctness.

2 Extensions and modifications

2.1 Vertical NQS effects

Vertical non-quasi-static (NQS) effects for minority charge and transfer current have been taken into account in HICUM from the very beginning. A second-order Bessel polynomial for ***both time and frequency domain analysis*** has been used along with an efficient implementation (Weil's approach [1]). Due to the conversion from FTN or C code to a Verilog-A implementation starting with version 2.21, the required access to the previous time steps became unavailable. The alternative of realizing the second-order differential equation through an adjunct network as in, e.g. VBIC, did not work initially, since this implementation is based on a bias *independent* transit time. With a bias dependent transit time, additional derivatives are generated that were shown by device simulation to be non-physical and, hence, undesired. As a consequence, it was recommended for version 2.21 and 2.22 that EDA vendors keep employing their existing Weil's approach based NQS code.

Most recently, an adjunct network implementation was found that avoids the undesired derivatives [2, 3] and which accurately matches the small-signal results obtained from the Bessel polynomial used in Weil's approach in version 2.1 (and earlier ones). This implementation is now available in version 2.23 and briefly described below.

Vertical NQS effects have been implemented in HICUM through "additional delay times" for both minority charge Q_f and forward transfer current i_{Tf}. These additional delay times are described as a function of bias by relating them to the transit time [4],

$$\tau_2 = \alpha_{Qf}\tau_f \quad \text{and} \quad \tau_m = \alpha_{iT}\tau_f. \tag{2.1.0-1}$$

The factors α_{Qf} and α_{iT} are model parameters.

Non-quasi-static behavior results from temporally and spatially distributed effects within the transistor structure. Therefore, theoretical treatment requires the solution of the continuity and transport equation. Under certain simplifications regarding the transistor structure and assuming small-signal operation, the corresponding second-order differential equation can be solved in one dimension and in frequency domain. Truncating the solution after the second frequency term reads

$$\underline{X}_{nqs} \approx X_{qs} - (\omega\tau_2)^2 - j\omega\tau_1 \text{ with } (X = I_T, Q_f), \tag{2.1.0-2}$$

which is valid at each bias point. X_{qs} is the corresponding quasi-static value; τ_1 and τ_2 are time constants, and ω is the radian frequency. Converting the frequency-domain solution X (= $\underline{I}_T$, $\underline{Q}_f$) to a slightly different form (with s = jω),

$$\frac{\underline{X}_{T,\,NQS}(\omega)}{\underline{X}_T} = 1 - s\tau_1 + (s\tau_2)^2 \cong \frac{1}{1 + A_1 s + A_2 s^2}, \tag{2.1.0-3}$$

which is valid for not too high frequencies, allows to apply Laplace transformation in order to obtain the corresponding time-domain approximation,

$$A_2 \frac{d^2 x_{T,\,NQS}}{dt^2} + A_1 \frac{dx_{T,\,NQS}}{dt} + x_{T,\,NQS} = x_T(t), \; x = (i_T, Q_f). \tag{2.1.0-4}$$

This transformation is always valid as long as the linearized small-signal case is also considered in time-domain. The form of the obtained 2nd-order differential equation resembles the existing time-domain solution. If (2.1.0-4) is interpreted as Bessel polynomial by simply choosing A_2 slightly differently from its expression that would result from (2.1.0-3), it was shown in [1] that the above system accomplishes in both domains the task of properly shifting the terminal currents as a consequence of NQS effects. The change of A_2 is correlated with A_1 and, thus, τ_1. As a consequence, only the first-order time constants ("delay times") are required for modeling. This is demonstrated in Fig. 2.1.0/1, in which (2.1.0-3) is compared to the small-signal results from 1D device simulation. The conversion $1\text{-}X \rightarrow (1+X)^{-1}$ in (2.1.0-3) along with the 2nd-order term enables the magnitude to follow the physically correct drop rather than to increase. The form $(1+X)^{-1}$ is in fact more accurate over a wider frequency range or, in other words, allows to compensate for ignoring higher order terms of the original physics-based solution. Note, that the impact of C_{jCi} on the results is negligible at the selected high current density bias point. This example shows that the above transformation system not only is consistent in frequency- and time-domain but also yields accurate results. For comparison, also the partitioned charge-based (PCB) model is shown with its incorrect description of both base current (i.e. input admittance) and magnitude of the collector current (i.e. transconductance).

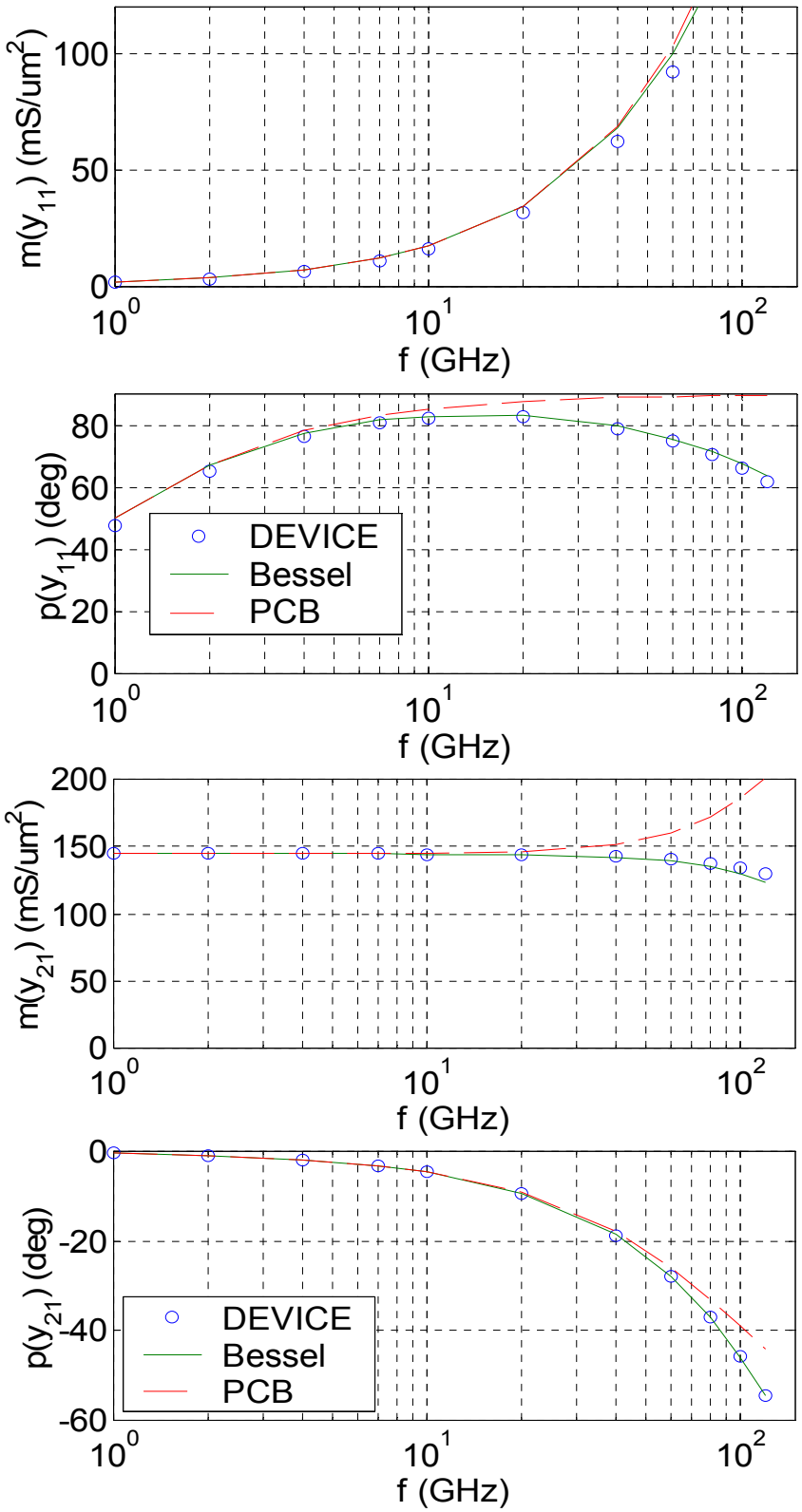

Fig. 2.1.0/1:Comparison of (2.1.0-3) with AC device simulation results for the a 100GHz SiGe HBT operated at $J_C = 6.1\text{mA}/\mu\text{m}^2$ ($V_{B'E'} = 0.922\text{V}$) and $V_{B'C'} = 0\text{V}$.

As shown in Fig. 2.1.0/2, the delay times, as calculated from device simulation, increase with bias current and are proportional to the transit time. Therefore, for each bias point, the proper delay time has to be inserted.

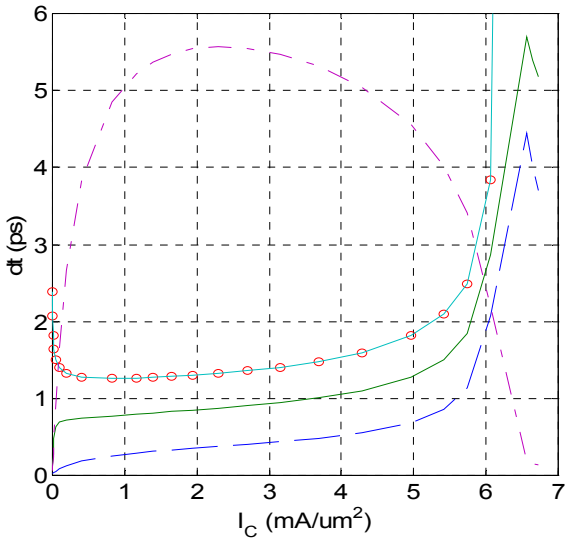

Fig. 2.1.0/2:NQS delay times τ_{IT} (solid green line) and τ_{Qf} (dashed blue line) vs. bias current for the CED HBT. For reference, the accumulated transit time $\tau_{m\Sigma}$ (line with circles) from Regional Analysis as well as f_T (dash-dotted red line) have been inserted.

For general large-signal operation no analytical solution exists. Observation from device simulation and measurements at medium and high-current densities for both sinusoidal and pulse signals with several 100mV amplitude indicates that there is no fundamental difference in the NQS behavior. In other words, the terminal currents react delayed w.r.t. the input voltage. Thus, the 2nd-order differential equation should still be applicable to accomplish the delay. In practice, transient simulation consists of a sequence of circuit equation system solutions at discrete time points. The change between time points is generally small enough to consider the theoretical solution as a sufficiently accurate representation, if just the time constants at each time (i.e. bias) point are inserted. In other words, the linearized delay transformation form (2.1.0-4) is applied to each time point. The accuracy of this approach has been demonstrated numerous times by examples ranging from device simulation to production circuit design.

The expression (2.1.0-4) can be implemented in a circuit simulator with an LCR network or its corresponding gyrator equivalent [5], as shown in Fig. 2.1.0/3. The gyrator network avoids inductors which is advantageous in certain circuit simulators.

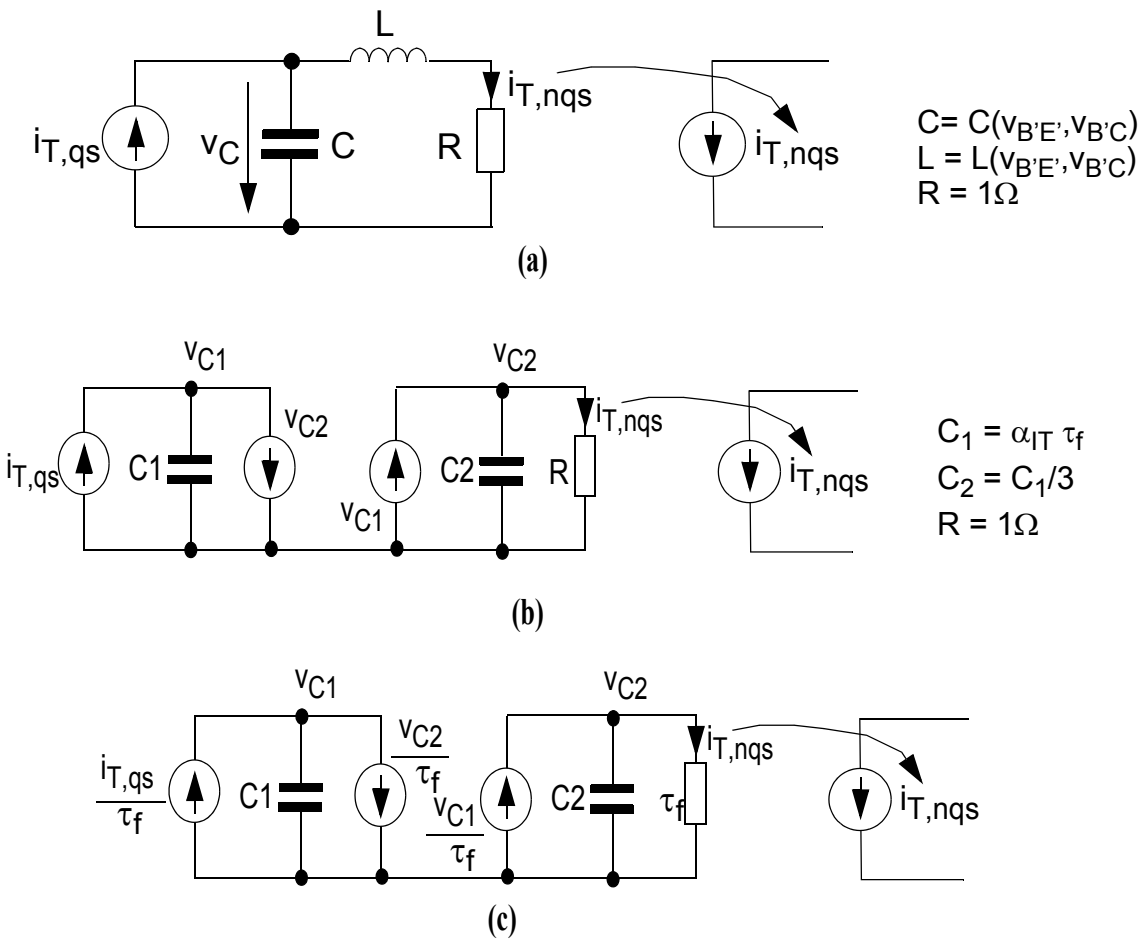

Fig. 2.1.0/3: (a) Adjunct LCR network for describing NQS effects of the transfer current i_T (a similar circuit holds for the minority charge Q_f); (b) Gyrator equivalent of LCR circuit in (a); (c) Gyrator equivalent circuit with normalization to the transit time in order to eliminate the undesired derivatives due to the bias dependence delay time.

Since the response of an LCR network represents a second-order polynomial exactly ***in time and frequency domain***, it has been selected for implementing ***NQS effects*** in HICUM via ***Verilog-A***, which does not permit the implementation via Weil's approach anymore. Unfortunately, a straightforward implementation is not possible since the bias dependence of the delay times causes the model compiler to create undesired derivatives in the small-signal network. Although these derivatives are mathematically correct, they simply result from a physically inadequate representation of the NQS effect through the adjunct network.

In order to overcome the derivative issue, the equations of the gyrator network had to be modified according to Fig. 2.1.0/3(c). Here, one can write in case of a bias dependent transit time τ_f the following equations

$$\left(\frac{I_{T,qs} - V_{C2}}{\tau_f}\right) = \frac{d}{dt}(\alpha_{IT} V_{C1}), \tag{2.1.0-5}$$

$$\left(\frac{V_{C1} - V_{C2}}{\tau_f}\right) = \frac{d}{dt}\left(\frac{\alpha_{IT}}{3} V_{C2}\right). \tag{2.1.0-6}$$

The above equations effectively make the capacitive elements bias-independent and, hence, remove the generation of undesired derivatives [6]. The same trick has been used for the corresponding minority charge related network.

As shown in Fig. 2.1.0/4 the overall equivalent circuit for HICUM/L2 has been extended with two adjunct networks for the NQS effects in i_T and for Q_f, respectively. It is important to mention that the original HICUM/L2 equivalent circuit has not been changed at all; i.e. the two adjunct networks have been added separately and are basically Verilog-A artifacts from the implementation point of view for NQS effects. They will only be evaluated if NQS effects are turned on using the parameter flag ***flnqs***.

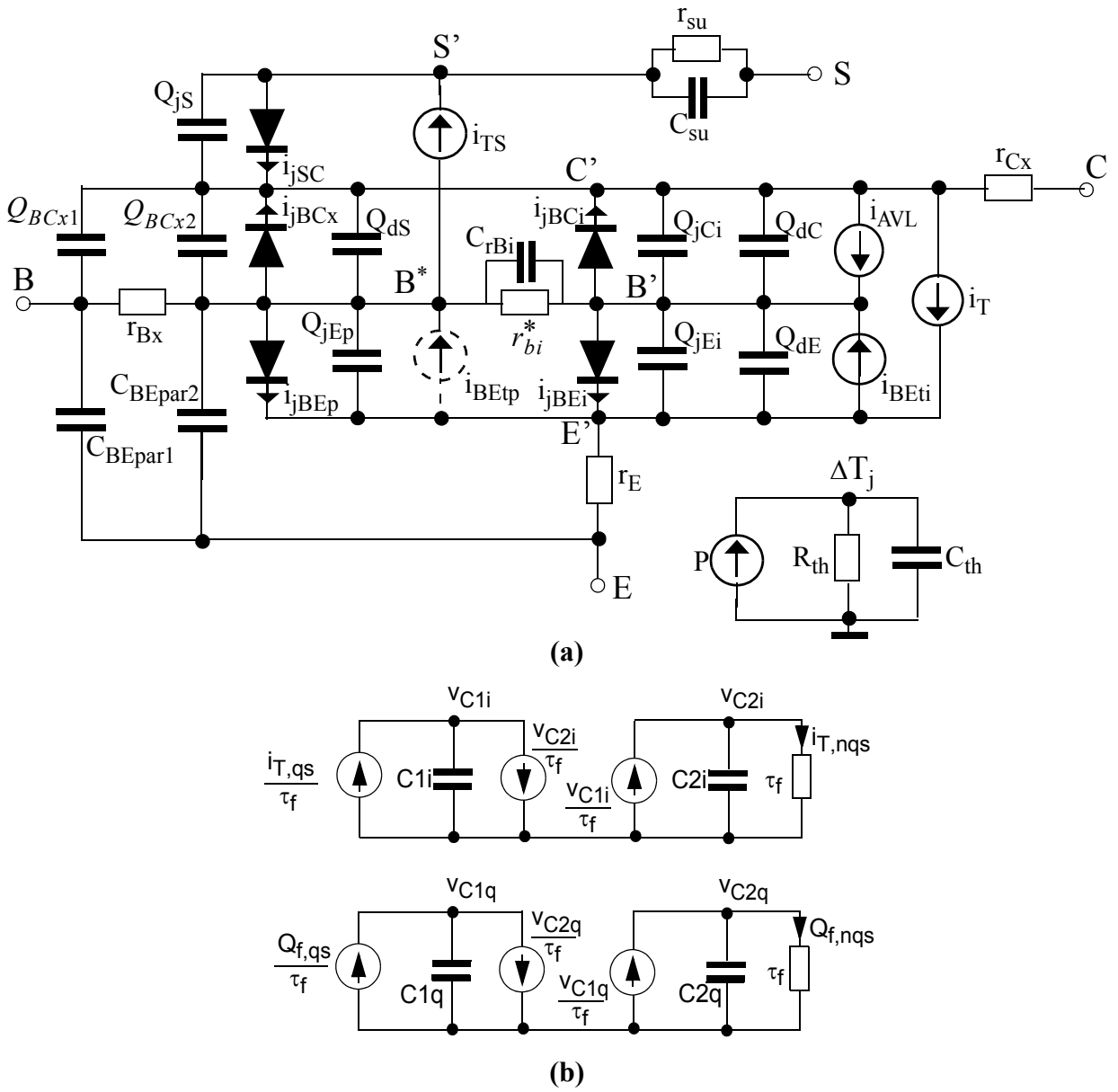

Fig. 2.1.0/4: (a) Existing large-signal HICUM/Level2 equivalent circuit with thermal network. (b) Adjunct NQS networks for transfer current i_T and minority charge Q_f, respectively.

The Verilog-A implementation of NQS effects has been verified against the built-in HICUM/L2 version 2.1 model in SPECTRE, which uses Weil's approach for the implementation. The following figures show the collector and base current waveforms for a 20ps pulse applied at the base of the transistor. As reference and to estimate deviations from possibly different time steppings during the transient, the quasi-static results have also been inserted. The plots are showing good agreement

for NQS results. Plot units are [A] for currents, [V] for voltages, [Hz] for frequency and [s] for time.

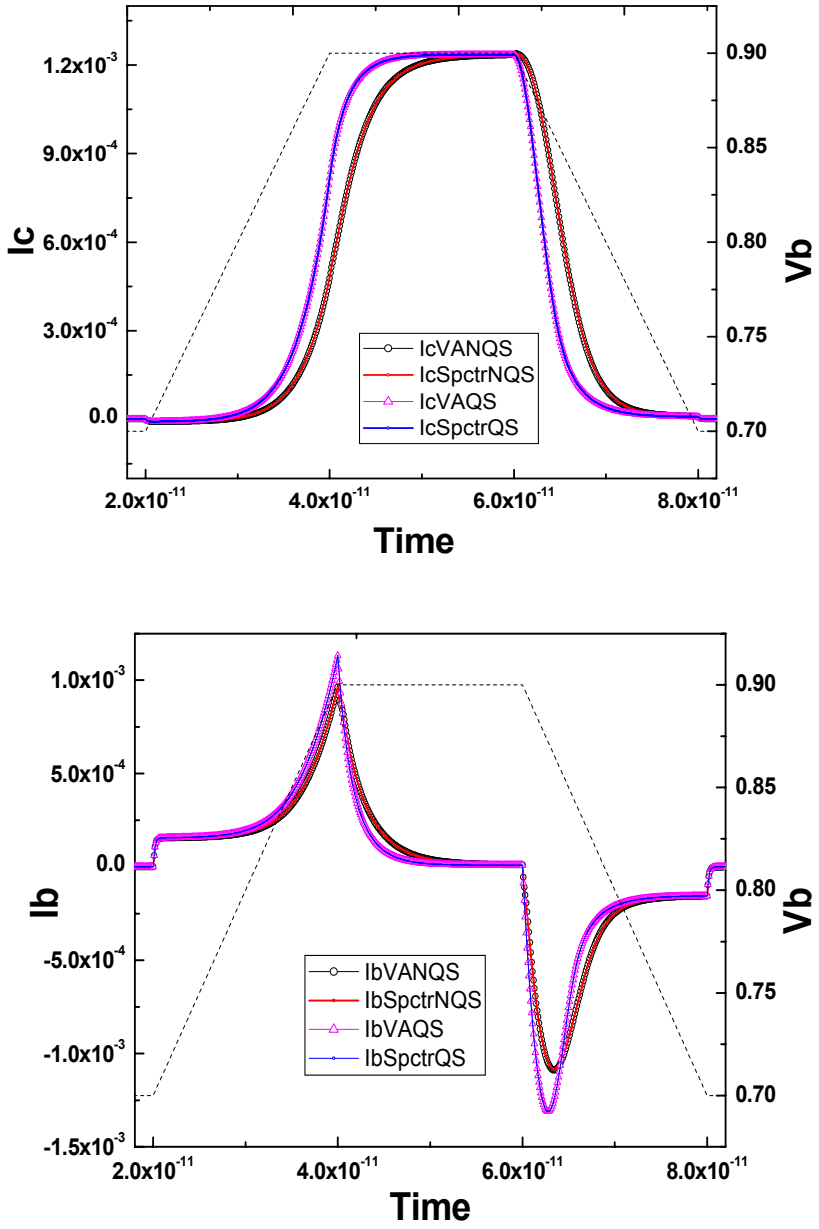

Fig. 2.1.0/5: Time dependence of the collector current (upper fig.) and base current (lower fig.) in response to a voltage input pulse (dotted line): comparison between v2.23 VA code with NQS networks (solid line with diamonds), v2.1 in SPECTRE with Weil's implementation (solid red line). For reference, the quasi-static results are also inserted for VA v2.23 (large diamonds) and v2.1 in SPECTRE (blue solid line).

Further testing has been performed using a smooth input pulse (rather than a ramp with its discontinuities) in order to rule out any time stepping related discrepancies. The time dependence of the pulse was calculated as

$$s(t) = S_{max}[1 - e^{-(t/\tau)^2}], \tag{2.1.0-7}$$

with the time constant

$$\tau = \frac{\sqrt{2/e}}{2\pi f} \quad , \tag{2.1.0-8}$$

where S_{max} is the maximum amplitude of the pulse and f is the frequency in Hz. The results in Fig. 2.1.0/6 show a very good agreement than for the ramp also. Note that for smooth signals the same accuracy as for discontinuous signals is obtained with a much smaller number of time points.

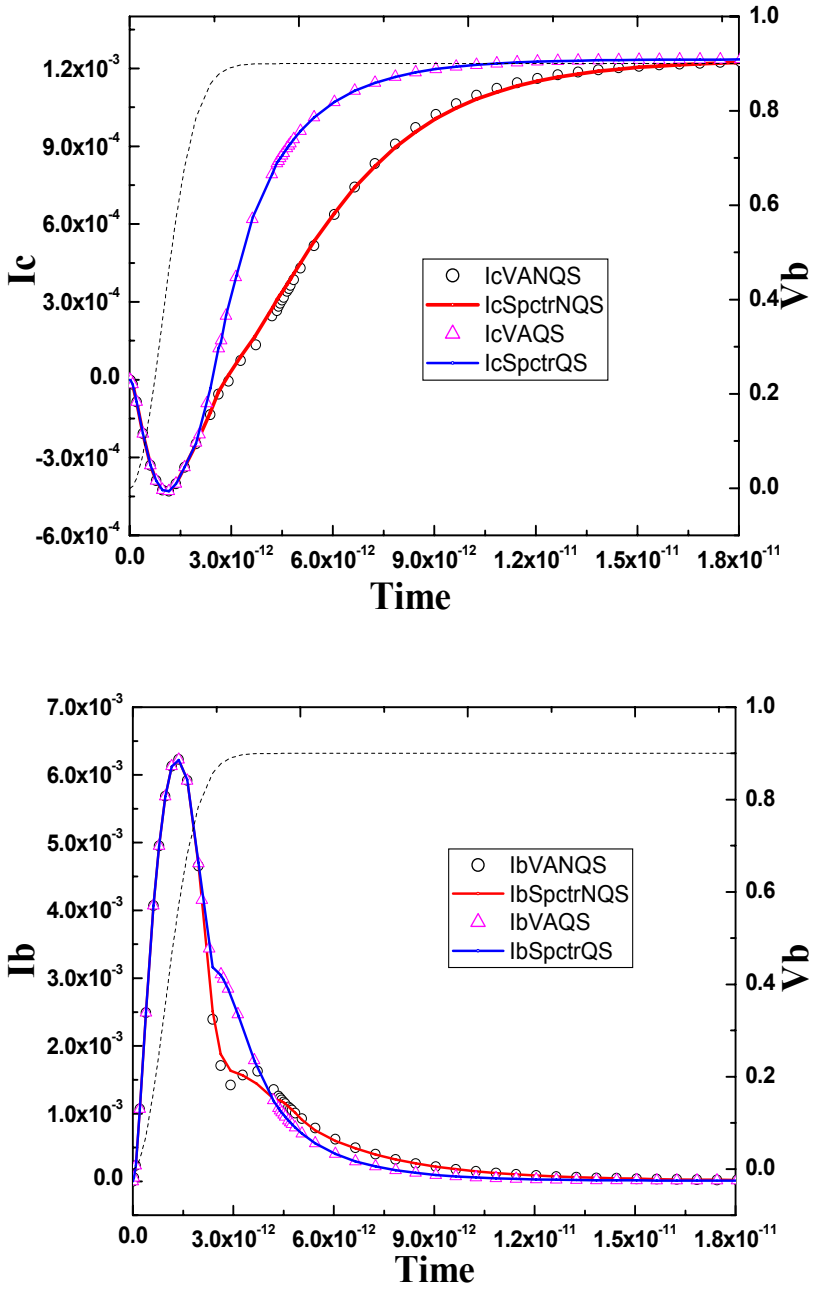

Fig. 2.1.0/6: Time dependence of the collector current (previous page fig.) and base current (current page fig.) in response to a smooth voltage input pulse (dotted line) with a maximum slope corresponding to a frequency of 100GHz: Comparison between v2.23 VA code with NQS networks (black circles), v2.1 in SPECTRE with Weil's implementation (solid red line). For reference, the quasi-static results are also inserted for VA v2.23 (triangles) and v2.1 in SPECTRE (blue solid line).

Frequency domain results in terms of small-signal y-parameters are shown in Fig. 2.1.0/7. As expected and desired, mostly the phase is altered by the NQS effects, and the magnitudes show the physically correct behavior. NQS effects have no impact on the inverse y parameters.

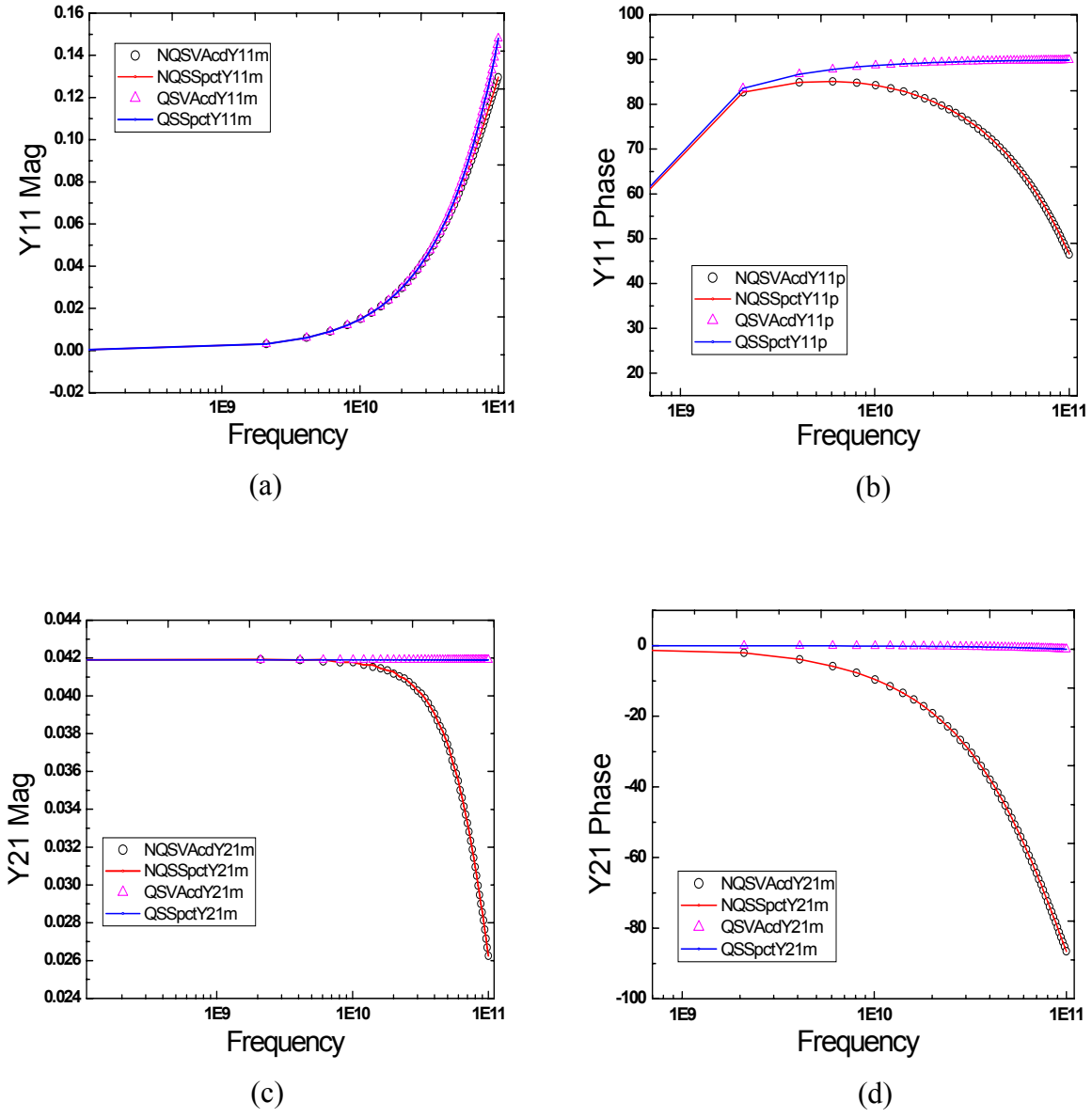

Fig. 2.1.0/7: Small-signal forward y-parameters for V_{BE} = 0.9V and V_{CE} = 0.9V: comparison between v2.23 VA code with NQS networks (diamonds), v2.1 in SPECTRE with Weil's implementation (solid red line). For reference, the quasi-static results are also inserted for VA v2.23 (triangles) and v2.1 in SPECTRE (blue solid line).

2.2 Lateral NQS effects

There has been a change in the expression for C_{rBi} compared to version 2.22. In the new expression, the contributions related to C_{dei} and C_{dci} have been included w.r.t. the proper node voltages.

$$C_{rBi} = f_{crBi}ddx(Q_{jEi}, V(bi)) + ddx(Q_{jCi}, V(bi)) \\ ((-1)ddx(Q_{dEi}, V(ei)) + (-1)ddx(Q_{dCi}, V(ci))) \tag{2.2.0-1}$$

and

$$Q_{rBi} = C_{rBi}V(bp, bi)\,. \tag{2.2.0-2}$$

It is still being recommended, according to theory, to turn on lateral NQS effects ***only for small-signal operation***.

2.3 Correlation between base and collector noise

In advanced SiGe HBTs the importance for taking into account the correlation between base and collector noise is increasing. Unfortunately, conventional SPICE-like circuit simulators do not include correlation between noise sources in their solution algorithm. Since EDA vendors are unlikely to change their noise simulation approach it is necessary to find an alternative way to take into account noise correlation in compact models. A working solution to do so was presented in [7]. Below, the implementation related information is summarized.

According to [7], the complex valued correlation factor $\underline{t}_{21}$ is given by

$$t_{21} = \frac{\underline{S}_{i_{nc}i_{nb}}}{S_{i_{nb}}} = -j\omega\frac{\tau_{Bf}}{3}\frac{I_T}{I_{jBEi}}\,. \tag{2.3.0-1}$$

Here, I_{jBEi} is the d.c. base current from emitter backinjection (intrinsic base emitter diode), I_T is the d.c. transfer current, τ_{Bf} is base transit time,

$$\underline{S}_{i_{nc}i_{nb}} \approx -2qI_T\left(j\omega\frac{\tau_{Bf}}{3}\right) \tag{2.3.0-2}$$

is the collector current noise spectral density related to the base current noise, and

$$S_{i_{nb}} = 2qI_{jBEi} \ , \ . \tag{2.3.0-3}$$

the base shot noise spectral density.

The negative sign in t_{21} makes the realization of the correlation in Verilog-AMS difficult to implement since in SPICE-like simulators the noise PSD is a squared quantity, leading to a cancellation of the negative sign. Hence, the following approximation is used,

$$S_{\underline{i_{nc}}} = S_{i_{nc}}\left(1 - B_f\left(\omega\frac{\tau_{Bf}}{3}\right)^2\right)^2 = S_{i_{nc}} - |t_{21}|^2 S_{i_{nb}} + \underbrace{\frac{|t_{21}|^4}{4B_f}S_{i_{nb}}}_{\text{error term}} \tag{2.3.0-4}$$

with B_f as d.c. gain, and the collector shot noise spectral density

$$S_{i_{nc}} = 2qI_T \ . \tag{2.3.0-5}$$

In equation (2.3.0-4), the factor 1/3 results from the same series expansion as for the transfer current related NQS effect in the base of a pure diffusion transistor. Therefore, the corresponding parameter “alit” is used instead of the factor 1/3.

Three shot noise sources have to be implemented - two for the transfer current and one for the base current. The transfer current related noise sources have to be implemented as controlled sources by tagging a capacitor (representing the noise correlation time) to the input noise source in order to obtain the frequency dependence. The corresponding equivalent circuit is shown in Fig. 2.3.0/1. The upper part contains the three noise sources while the two networks in the lower part of the figure are used for realizing the correlation expression. The equations for the three noise sources read:

$$I(bi, ei) = gV(b\_n1), \quad V(b\_n1) = \frac{1}{g}\sqrt{2 \cdot q \cdot i_{bei}}, \tag{2.3.0-6}$$

$$I(ci, ei)_1 = \left(1 - \frac{B_f}{2}(alit \cdot Tf \cdot \omega)^2\right) \cdot g \cdot V(b\_n2), \tag{2.3.0-7}$$

$$I(ci, ei)_2 = -j\omega \cdot B_f \cdot alit \cdot Tf \cdot g \cdot V(b\_n1), \ V(b\_n2) = \frac{1}{g}\sqrt{2 \cdot q \cdot i_t}. \tag{2.3.0-8}$$

$I(ci,ei)_2$ indeed represents the negative contribution caused by the correlation while $I(ci,ei)_1$ includes the (undesired) error term resulting from the approximation (2.3.0-4).

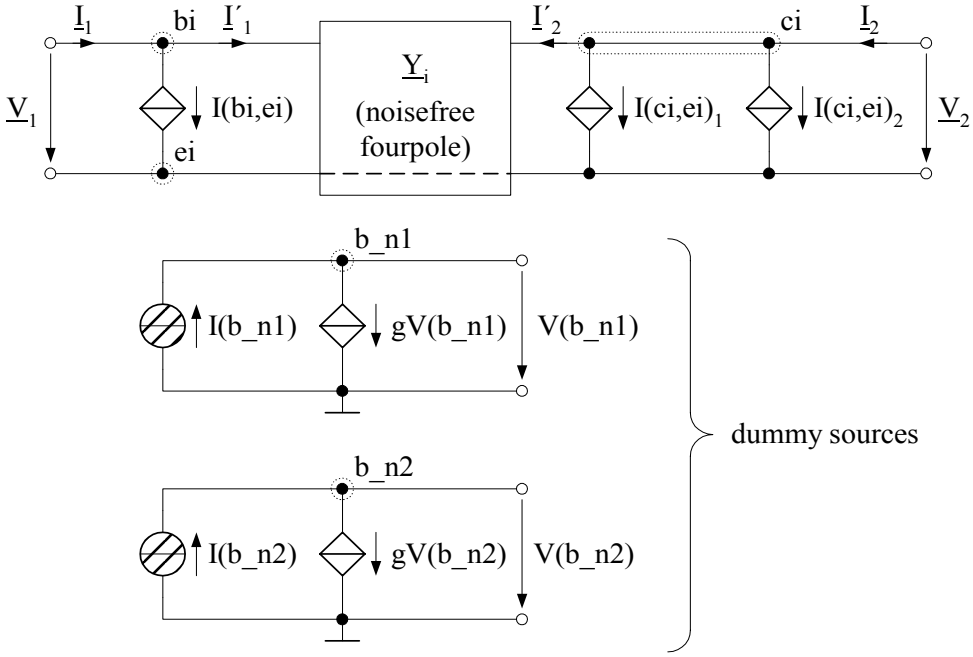

Fig. 2.3.0/1:Equivalent circuit used for implementing noise correlation. The lower two networks (labelled as dummy sources) are used for realizing the correlation.

The implementation was experimentally verified on SiGe HBTs. To provide a feeling for the relevance of correlated noise and the accuracy of the implemented noise correlation model, examples are shown in Fig. 2.3.0/2 and 2.3.0/3 for a SiGe HBT with peak transit frequency of 150GHz (emitter area 0.2*10.16μm^2, CBEBC configuration). The correlation has its biggest impact on the minimum noise figure NF_{min} and the real part of the optimum source reflection coefficient Γ_{opt}. The importance of the correlation increases with frequency. The results show that HICUM with the implemented noise correlation agrees quite well with measured data. Note that the error term in (2.3.0-4) results in a limitation of the accuracy of this implementation to not too “high” frequencies.

It is to be mentioned that, the noise correlation code section has been tested and works well with the Tiburon compiler, but not with ADMS. This is due to the fact that the respective VA code section combines more than one analog expression with binary operators, which presently still a restriction in ADMS. This restriction is expected to be removed in a future version of ADMS [8].

Hence, it is being advised to turn-off (by front slash "//") the noise correlation code section for simulation with Spectre.

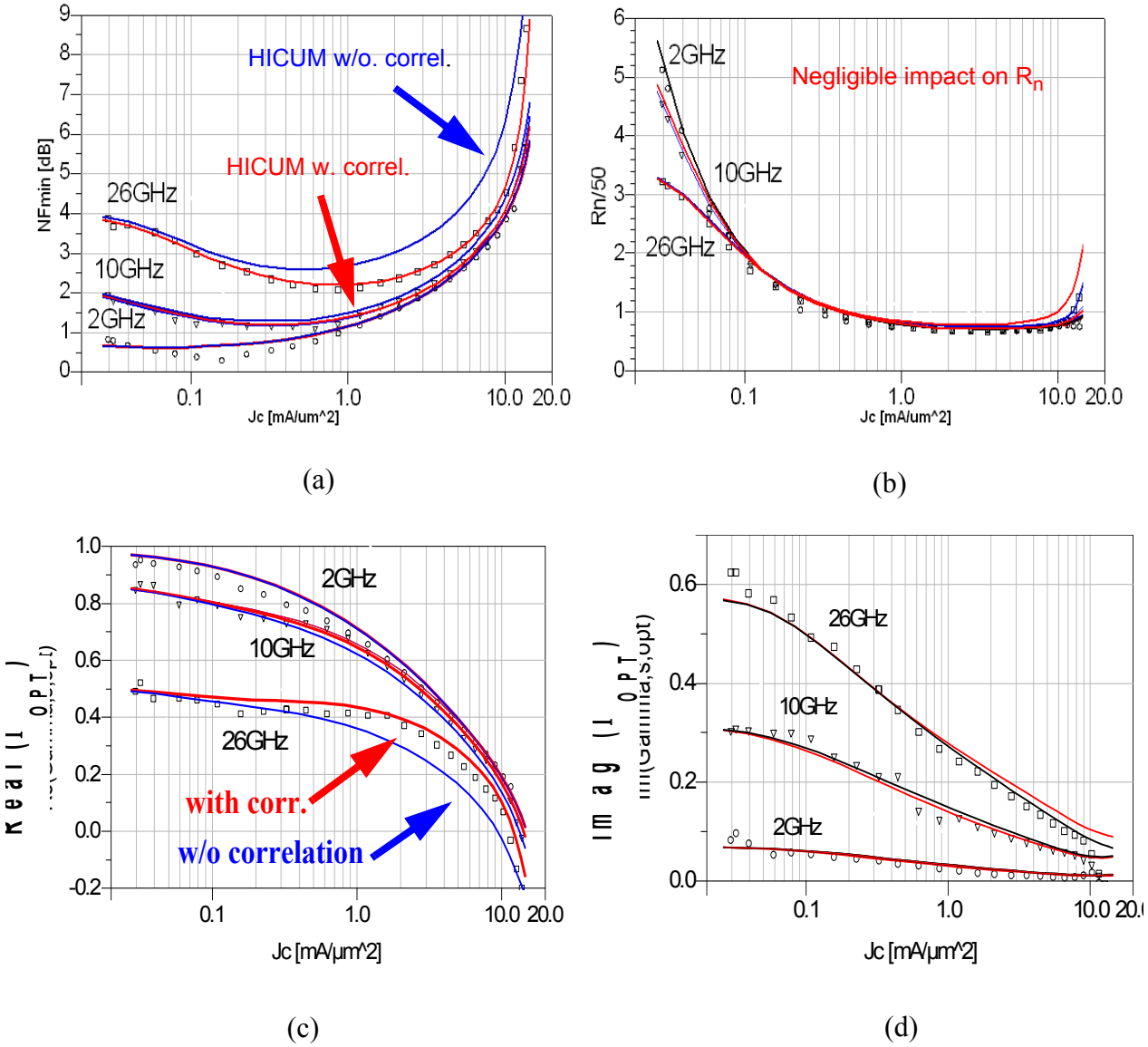

Fig. 2.3.0/2: Comparison of measured noise parameters (symbols) with simulated data from HICUM without correlation (blue lines) and with correlation (red lines). (a) Minimum Noise factor; (b) Equivalent noise resistance; (c), (d) real and imaginary part of optimum source reflection coefficient. The hardware was provided by Jazz Semiconductor.

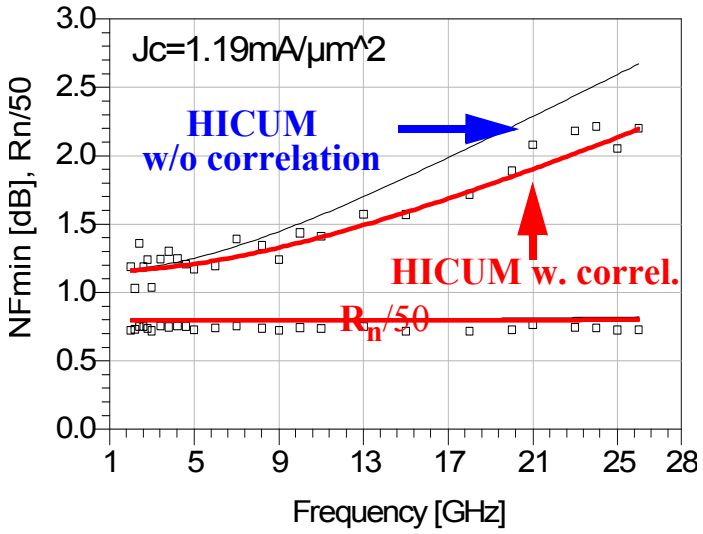

Fig. 2.3.0/3: Frequency dependence of NF_{min} and R_n at the optimum bias point in terms of noise.

2.4 Collector current spreading

Version 2.22 contains the function

$$FC\ln l \;=\; \ln(1 + latl \times FCw) \quad \text{for } latb > 0.01\,. \tag{2.4.0-1}$$

For a very small argument, a series expansion was used, which was implemented as

$$FC\ln l \;=\; latl \times FCw \quad \text{for } latb \le 0.01\,. \tag{2.4.0-2}$$

Fig. 2.4.0/1 shows the amount of error in the range around latb = 0.01 using the approximation (2.4.0-2). Although values of latb = 0.01 are physically unlikely, the approximation (2.4.0-2) has been removed in version 2.23 and (2.4.0-1) is now being used for the entire value range. *The function (2.4.0-1) has been coded inside the HICFCI and HICFCT macro in order to improve the consistency.* The same has been done for the expression, $FC\ln b \;=\; \ln(1 + latb \times FCw)$.

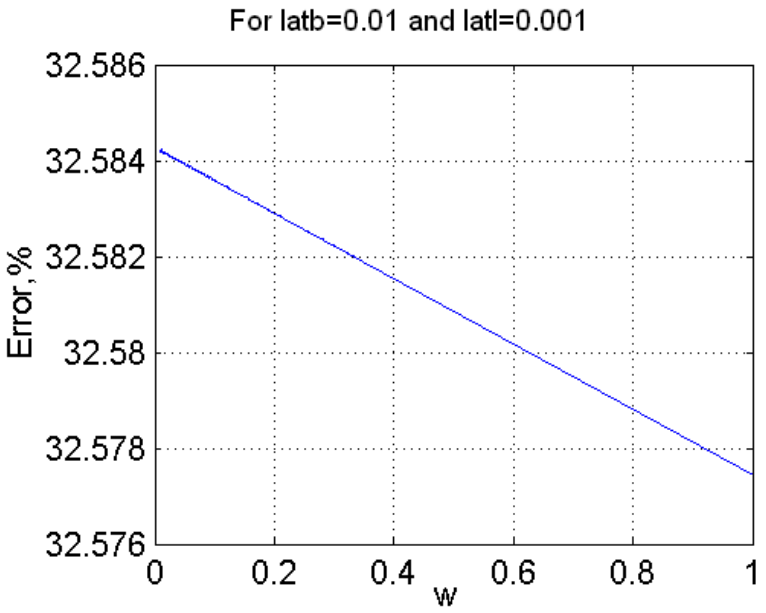

Fig. 2.4.0/1:Plot showing the percentage error (for latb=0.01 and latl=0.001) with normalized injection width, w.

2.5 Other small bug fixes

In the initial model (initial_model) section, the external if-block for HICTUN_T has been removed since it attempted to access the voltages V(bp,ei) and V(bi,ei) in that section. This avoids extra undesired and unnecessary iterations.

Two more small bugs that are also related to series expansions in procedures of the collector current spreading function have been fixed in the macro HICFCI and HICQFC as shown below. The new fixes are highlighted in red colour.

- Macro: HICFCI:
  - Old version:

```
a = z*z;
a2 = 3.0+z-0.5*a+z*a;
a3 = -2.0*z+1.5*a+2.0*a*a/3.0;
hicfcio = (zb*a2+zl*a3)*w*w/6.0;
dhicfcio_dw = z+0.5*a-a*z/3.0+5.0*a*a/6.0+zl*w*(a-z+2.0*a*a/3.0);
```

  - New Version:

```
a = z*z;\
a2 = 3.0+z-0.25*a+0.10*z*a;
a3 = 2.0*z+0.75*a-0.20*a*z;
hicfcio = (zb*a2+zl*a3)*w*w/6.0;
dhicfcio_dw = (1+zl*w)*(1+z)*lnzb;
```

- Macro: HICQFC
  - Old version:

```
FCd_a = 1.0/(1.0-FCf1*latb);
FCw = FCf1*FCd_a;
FCdw_daick = -1.0*FCd_a*FCd_a\
```

  - New version:

```
FCd_a = 1.0/(1.0+FCa_ck*latb);
FCw = FCf1*FCd_a;
FCdw_daick = -1.0*FCd_a*FCd_a*FCxb*FCd_a;
```

3 Comments on model release

3.1 Code

Reference code of the new HICUM version 2.23 has been made available in Verilog-A on the website,

http://www.iee.et.tu-dresden.de/iee/eb/eb_homee.html

Using a Verilog-A model compiler, C-code can be provided as well. It is expected that the updated model version will also be available in SPICE3F code [9] (please contact Prof. Jean-Claude Perraud at perraud@ecole.ensicaen.fr).

Depending on the future development and availability of model compilers, it is possible that future releases for HICUM can be provided directly as code for specific circuit simulators (i.e. those ones for which the compilers are setup to generate code). Such releases can possibly include model features that are special to the process technologies of cooperation partners for preliminary testing before being proposed for a release or being released in the standard version.

3.2 Model parameters

The model parameters in Table 3.2.0/1 have been reassigned new ranges in the new version

name	description	default	Old range	New range	test	unit
FGEO	Factor for geometry dependence of emitter current crowding	0.6557	[0:1]	[0:inf]	0.73	-
FDQR0	Correction factor for modulation by B-E and B-C space charge layer	0.0	[0:1]	[-0.5 :100]	0.2	-

Table 3.2.0/1:Summary of model parameter range changes with respect to version 2.22.

4 Frequently asked questions

4.1 HICUM names in simulators

The Table below contains a list of various circuit simulators and the respective command to call HICUM.

simulator name	call
ADS	HICUM
ELDO	Level = 9
HSPICE	Level = 8
SPECTRE	bht
APLAC	HICUM
AnalogOffice	HICUM_L2 (npn) , HICUM_L2_P (pnp)
Silvaco SPICE	Level = 6
NEXXIM	HICUM
Smart-SPICE	libHICUM
GoldenGate	HICUM

Table 4.1.0/1: HICUM model call convention in circuit simulators.

5 References

[1] P.B. Weil and L.P. McNamee "Simulation of excess phase in bipolar transistors", IEEE Trans. Circ. Syst., Vol. 25, pp. 114-116, 1978.

[2] M.Schroter, A.Mukherjee, “HICUM-productization and support update”, October CMC meeting, Boston, 2007.

[3] M.Schroter, A.Mukherjee, “HICUM-productization and support update”, March CMC meeting, Portland, 2008

[4] A. Koldehoff, M. Schröter, and H.-M. Rein, "A compact bipolar transistor model for very-high-frequency applications with special regard to narrow stripes and high current densities", Solid-State Electron., Vol. 36, pp. 1035-1048, 1993.

[5] Colin C. McAndrew,et al, “BJT Modeling with VBIC, Basics and V1.3 Updates”, and private communication, 2007.

[6] G. Coram, private communication, 2007.

[7] P. Sakalas, A. Chakravorty, J. Herricht, M. Schroter, "Compact Modeling of High Frequency Correlated Noise in HBTs”, Proc. Bipolar Circuits and Technology Meeting (BCTM), Maastricht (Belgium), pp. 279-282, 2006.

[8] G. Coram, “How to (and how not to) write a compact model in Verilog-A”, Proc. IEEE International behavioral modeling and simulation conference, pp. 97-106, 2004.

[9] For access to SPICE3.F with HICUM, please contact Prof. Jean-Claude Perraud at perraud@ecole.ensicaen.fr.